Polysaccharide-protein multilayers based on chitosan-fibrinogen assemblies for cardiac cell engineering

Maria Kitsara, George Tassis, Aristeidis Papagiannopoulos, Alexandre Simon, Onnik Agbulut, Stergios Pispas

Polysaccharide-protein multilayers based on chitosan-fibrinogen assemblies for cardiac cell engineering

Maria Kitsara[*]*, George Tassis, Aristeidis Papagiannopoulos*[*]*, Alexandre Simon, Onnik Agbulut*[1]*, Stergios Pispas*[2]

Dr. M. Kitsara, Mr. A. Simon, Prof. O. Agbulut
Sorbonne Université, Institut de Biologie Paris-Seine, CNRS UMR 8256, INSERM ERL 1164, Biological Adaptation and Ageing, Paris, 75005, France
* kitsara.m@gmail.com

Mr. G. Tassis, Dr. A. Papagiannopoulos, Dr. S. Pispas
Theoretical and Physical Chemistry Institute, National Hellenic Research Foundation, 48 Vassileos Constantinou Avenue, Athens, 11635, Greece
* apapagiannopoulos@eie.gr

Mr. G. Tassis
Department of Physics, University of Patras, 26504 Patras, Greece

Keywords: polysaccharide-protein multilayers**,** chitosan-fibrinogen assemblies, tunable hydrophilicity/hydrophobicity, cell-material interaction, cardiomyocytes culture

Abstract

The cell and tissue culture substrates play a pivotal role in the regulation of cell-matrix and cell-cell interactions. The surface properties of the materials control a wide variety of cell functions. Amongst various methods, layer-by-layer (LbL) assembly is a versatile surface coating technique for creating controllable bio-coatings. Here, polysaccharide/protein multilayers are proposed, which are fabricated by immersive LbL assembly and based on the chitosan /fibrinogen pair for improving the adhesion and spreading of cardiomyocytes. Two approaches in LbL assembly are employed for clarifying the effect of the bilayers order and their concentration on cardiomyocytes viability and morphology. Fourier transform infrared spectroscopy (FTIR) measurements show that the adsorption of the biopolymers is enhanced during the LbL deposition in a synergistic manner. Contact angle measurements indicate that the multilayers are alternating from less to more hydrophilic behavior depending on the biopolymer that is added last. Confocal microscopy with immunostained fibrinogen reveals that the amount of the protein is higher when the concentration of the immersion solution is

increased, however, for low solution concentration it is speculated that interdigitation between the separate biopolymer layers takes place. This work motivates the use of fibrinogen in polysaccharide/protein multilayers for enhanced cytocompatibility in cardiac tissue engineering.

1. Introduction

One of the critical aspects of biomaterials for tissue engineering and regenerative medicine is their ability to control cell functions such as adhesion, morphology, migration, differentiation and proliferation. The surface properties of biomaterials and generally tissue culture substrates play a pivotal role in the regulation of cell-matrix and cell-cell interactions [1]. Therefore, surface functionalization with biomimetic coatings is of paramount importance towards the direction of resembling the extracellular matrix microenvironment. In specific, coatings with natural biopolymers have the advantage of possessing the necessary biochemical cues for cells attachment and at the same time their degradation products are non-toxic and have a low immune response [2].

Various methods for surface functionalization with biomimetic coatings have been employed, but layer-by-layer (LbL) assembly consists of a versatile and low-cost coating technique leading to controllable bio-coatings. [3]. In this technique, polyelectrolyte multilayers (PEMLs) are fabricated that consist of alternating anionic and cationic polymers in aqueous media that self-assemble on an interface driven by electrostatic interactions [4],[5]. This way, stable films with high adsorbed amounts can be obtained whereas in simple adsorption of a single polyelectrolyte the effect would be weak [6]. Protein-polyelectrolyte (or polysaccharide) complexation can be used to introduce the versatility of proteins regarding their pH-dependent charge distribution and patchy hydrophobic surface [7,8]. Recently the multilayer formation between polyelectrolytes and protein/polyelectrolyte complexes was proposed as a method for stable multilayers [9,10]. PEMLs are proposed for applications related to tissue engineering [11,12],

drug delivery [13] and cell culture in general [14–17]. LbL self-assembled PEMLs have effectively maintained the concentration of a growth factor for cell cultures to avoid repeated growth factor addition and intervention [14]. Interdigitation between the polyelectrolytes in PEMLs has been suggested as a modulating factor for cell adhesion [15] and cell morphology and growth [18].

Even though LbL assembly is a well-known technique, the combination of materials for assembling functional coatings for cardiac tissue engineering has not yet been explored. In this work we propose polysaccharide/protein multilayers (PPMLs) based on the chitosan (Chit)/fibrinogen (Fbg) pair in order to improve the adhesion and spreading of cardiomyocytes in culture. Chit as a polysaccharide is biodegradable, biocompatible and non-toxic [19], and has been used in tissue engineering and cell growth studies in the form of hydrogels [20], films [21,22] and nanoparticles [23]. Fbg is a blood plasma protein and has the ability to polymerize into fibrin and in this way plays a major role in blood clotting and platelet aggregation [24]. Its active sites allow for binding fibroblasts, endothelial cells and their growth factors [25,26]. Micro- and nanostructured Fbg-based biomaterials have shown potential for the delivery of drugs, biomolecules and genes in tissue engineering applications [27]. In this work, we employed LbL deposition of five bilayers of Chit/Fbg in order to create stable films that can support the culture of cardiomyocytes. We studied the effect of the layers' order as well as of their concentration on the cardiomyocytes attachment and spreading. Therefore, we deployed PPMLs where the top layer, which was in contact with the cells, in one case was Fbg and in the other case Chit. Then the effect of their concentration on cell adhesion and spreading was evaluated by using two different concentrations for both Chit and Fbg.

2. Results and Discussion

2.1. PPMLs physicochemical characterization

Fbg has a well-documented trinodular structure. It consists of three nodules (D-E-D domain), which are connected by two triple-stranded amino-acid helices [28]. The two-end αC domains interact electrostatically with the central E domain in a manner that is pH-dependent [29]. E and

D domains are negatively charged at neutral pH and positively charged at acidic pH (below 3.5). αC domains are positively charged at both neutral and acidic pH as they contain arginine and lysine residues. Therefore, near Fbg's isoelectric point (pI=5.5-5.8) Fbg contains domains of both negative (E and D) and positive (αC) charge [30,31]. The αC domains of Fbg are hydrophilic while E and D domains are hydrophobic [32,33]. Adsorption of Fbg and plasma proteins on solid surfaces has been thoroughly investigated because it is very crucial for the interaction of blood plasma with biomaterials [34,35]. Fbg can adsorb on hydrophilic surfaces by electrostatic interactions and to hydrophobic surfaces by anchoring its hydrophobic groups.

FTIR experiments were performed on PPMLs deposited on gold-coated surfaces. This was done because glass lamellae would not support the mechanical stresses from the ATR tool press and more importantly did not provide adequate reflection of light for ATR detection. Although the substrate used was not the actual substrate where the ML films for cell culture were formed, the synergistic accumulation of the two biopolymers and the interactions with each other in the formed films, can be characterized. In addition, it can be assumed that the top layers of both the MLs either on glass or on gold, which are away from the solid/water interface, have similar properties. Adsorption from separate pure solutions on gold surfaces is expected due to hydrophobic moieties on Chit [36,37] (hydrophobic content of Chit affects its interactions even at high degrees of deacetylation) and Fbg [32]. Experiments with pure Fbg solutions have shown that 5 min of adsorption is enough to reach adsorbed amounts higher than 10 mgm^{-2} on gold even for 0.1 $mg.ml^{-1}$ solution concentration [38]. More importantly, at times longer than 5 min adsorption kinetics is greatly slowed down as adsorption proceeds towards plateau coverage. Therefore, the multilayer deposition approach is expected to effectively increase the immobilized amount of Fbg as it exploits the Chit/Fbg interactions.

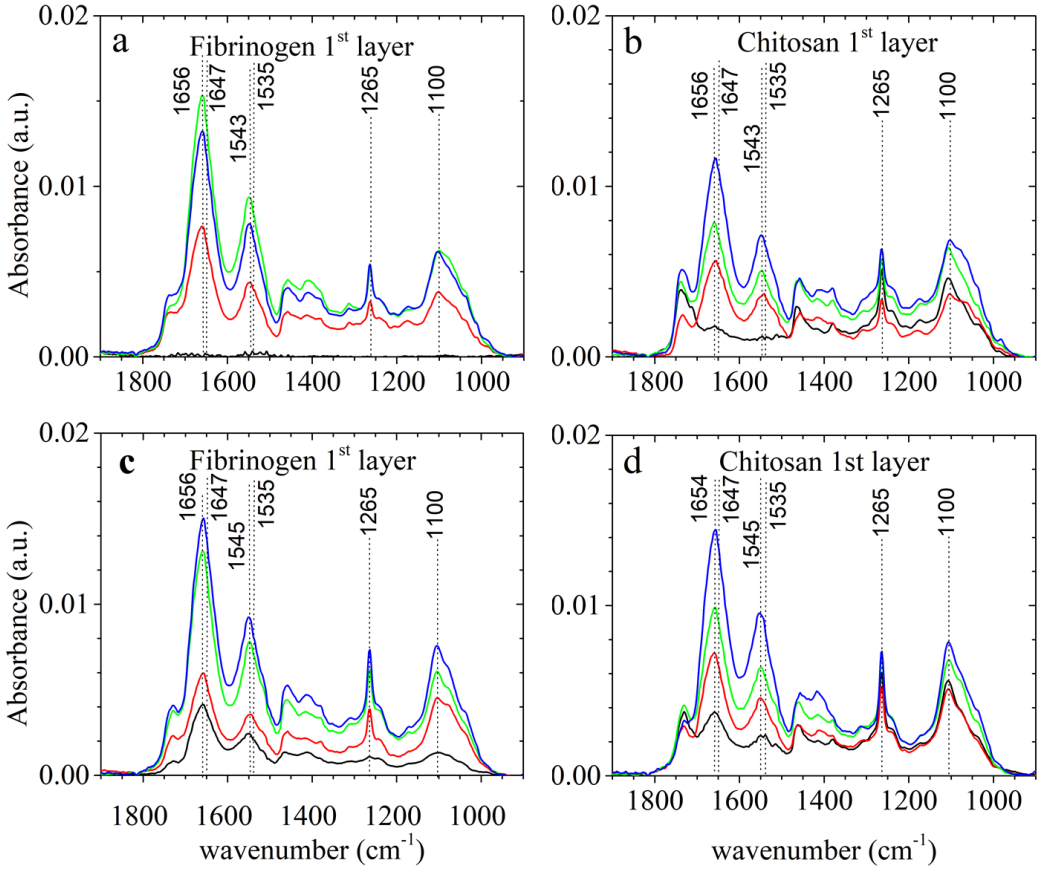

Figure 1. ATR-FTIR spectra at 1st (black), 2nd (red), 9th (green) and 10th (blue) stage of the sequential adsorption of 0.1 mg.ml^{-1}: Fbg (a), Chit (b) as the first layer and 1.0 mg.ml^{-1}: Fbg (c), Chit (d) as the first layer of polysaccharide/protein multilayers (PPMLs).

The characteristic bands of adsorbed Fbg and Chit are found in **Figure 1a and c** and **Figure 1b and d** respectively as first layers. There is a distinctive region at about 1100 cm^{-1} where Chit's characteristic groups absorb [39–41]. Fbg characteristic bands amide I and II are found at 1652 and 1541 cm^{-1} respectively [42,43]. Chit's amide II bending (1647-1650 cm^{-1}) and N-H bending (1535 cm^{-1}) are compatible with the FTIR spectra although they are near Fbg' amide I and II bands [44,45]. The characteristic bands generally increase in intensity upon successive depositions, which shows the multilayer build-up. It has to be noted that this was not an in-situ experiment but nevertheless measurements were taken on at least 3 different spots of the gold surface to confirm homogeneity and reproducibility. In any case, it is informative to discuss the evolution of separate regimes of the spectra. The increase in absorbance at e.g. 1100 cm^{-1} is possibly related to adsorbed Chit, because Fbg does not show any strong characteristic

absorption in the region 1200-1000 cm^{-1} (Figure 1). Sequential adsorption on preformed layers of Fbg is especially evident in Fig. 1c. Enhancement at 1100 cm^{-1} is observed from the 1st to the 2nd layer and from the 9th to the 10th layer (corresponding to Chit addition). This effect is not found in **Figure 1 b and d** where Fbg is the added 2nd and 10th layer. At the same time the increase in the amide I and II bands of Fbg is not so strong when Chit is added (2nd and 10th stage in **Figure 1a and c**) in comparison to the case when Fbg is added (2nd and 10th stage in **Figure 1b and d**). This is because these peaks appear relatively weaker in Chit (**Figure 1b and d**, 1st layer) in comparison to Fbg (**Figure 1c**). A band at 1265 cm^{-1} that appears only when Chit is present in the layers can be attributed to characteristic CH_2 wagging vibrations and combined N-H deformation and C-N stretching [45,46]. This band increases as more Chit is added on the layers. Therefore, ATR-FTIR experiments show that sequential adsorption of the two biopolymers effectively increases their adsorption on a surface in a synergistic manner and can be used to create multilayers on other surfaces too.

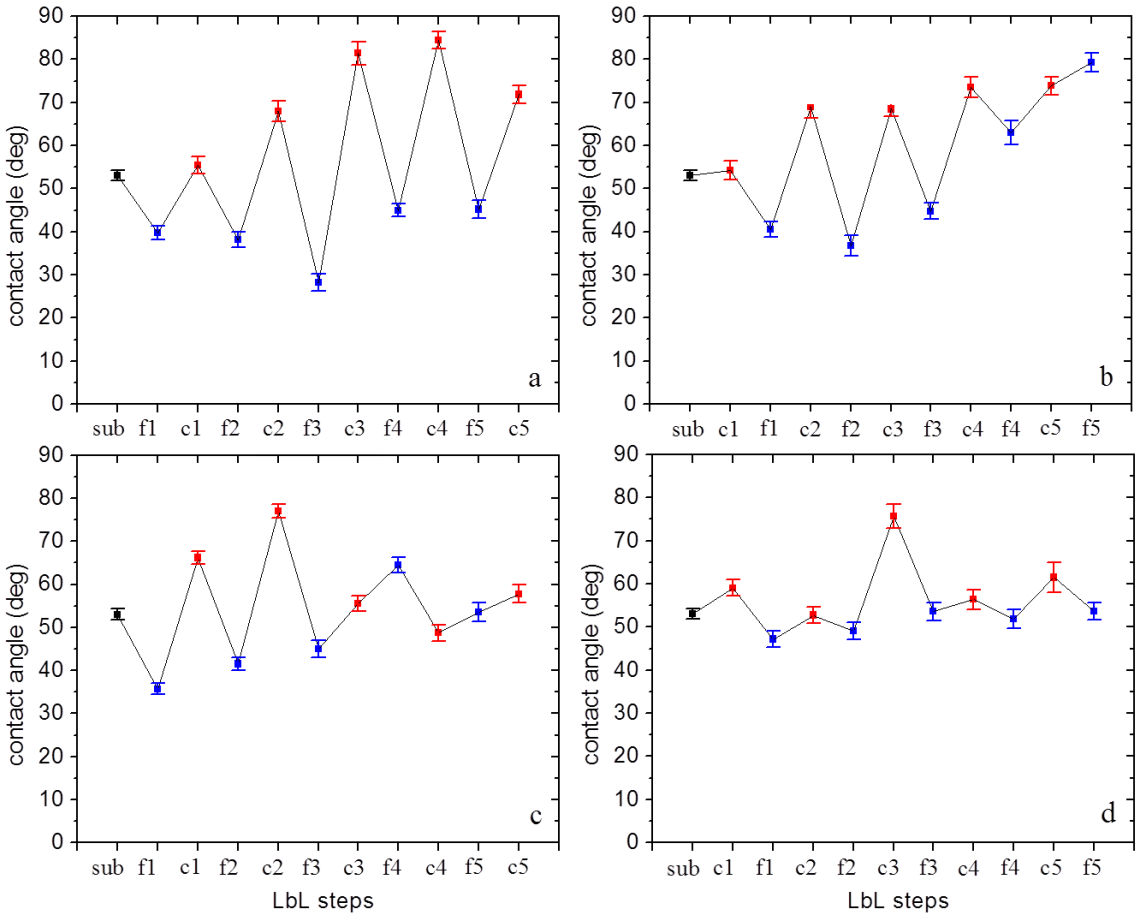

Figure 2. Contact angle from Chit (red)/Fbg (blue) MLs on glass substrate (black) from solutions of 0.1 mg.ml^{-1}: Fbg (a), Chit (b) as the first layer and 1 mg.ml^{-1}: Fbg (c), Chit (d) as the first layer of polysaccharide/protein multilayers (PPMLs).

Fbg is expected to adsorb strongly on glass surfaces at pH values both below and above its pI because it contains positively charged groups that may anchor to the negative charges on the glass/water interface [31,47]. Adsorption times shorter than 1 min are enough for Fbg adsorption on hydrophilic SiO_2 surfaces at neutral pH [48]. Glass surfaces maintain their negative surface charge at pH values down to 2 [31]. Adsorption of cationic polymers on glass surfaces is driven by the negative surface charge of glass when in contact with water [49], while Chit remains positively charged up to pH 6.5 [50].

Contact angle (CA) experiments provide straight-forward observation of the wettability properties of surfaces. In **Figure 2** the LbL formation of Chit/Fbg MLs is followed by CA measurements. The CA on clean glass lamella was CA= 53±2° which is compatible with literature results [51,52]. At low solution concentrations (0.1 mg.ml^{-1}) when Fbg is the first

component, adsorption and layer formation on the glass/water interface changes CA significantly (**Figure 2a**). CA drops towards lower values pointing to a more hydrophilic interface. The hydrated layer of adsorbed Fbg is hydrophilic, apparently due to the dissociated Fbg groups. The CA value of about 40° is compatible with the value measured for hydrated Fbg films on glass i.e. 46.5° [53]. Applying the Chit solution leads to an increase in CA (**Figure 2a**). This tendency towards hydrophobic behavior comes from the fact that Chit interacts electrostatically with the pre-adsorbed Fbg. Upon neutralization of the negative charges of Fbg's E and D domains their hydrophobic nature is more pronounced. In addition, neutralization of Chit monomers makes its chain more hydrophobic due to the presence of methyl groups [54–56]. Alternating Chit and Fbg layers lead to a saw-tooth pattern with successive changes from less to more hydrophilic behavior respectively.

The situation is very similar when Chit is the first layer (**Figure 2b**). Nevertheless, application of the Chit 0.1 mg.ml^{-1} solution on bare glass lamella has no significant change on the CA, indicating its low initial adsorption. However, the saw-tooth pattern follows similarly to Fig. 2a after the application of Fbg solution. Consequently, alternating Chit with Fbg leads successively to more hydrophobic or more hydrophilic layers (respectively) either if Chit or Fbg is the first solution applied on the glass surface. In more detail, when Fbg is the first layer the mean CAs for Chit and Fbg as top layers are 72°±12° and 39°±7° respectively whereas for Chit as a first layer the values are 68°±7° and 53°±17° (**Figure 2a and b**).

For solutions of high concentration (1 mg.ml^{-1}) (**Figure 2c and d**) a saw-tooth pattern is also followed, at least for 6 layers when Fbg is the first layer (**Figure 2c**), and for all 10 layers when Chit is the first layer although with a weaker intensity (**Figure 2d**). When Fbg is the first layer the mean CAs for Chit and Fbg as top layers are 61°±10° and 48°±11° respectively whereas for Chit as a first layer the values are 61°±8° and 51°±3° (**Figure 2c and d**). In conclusion, the hydrophilicity/hydrophobicity of the mixed layers can be tuned by choosing one of the two

components as the outermost component (especially by adsorption from solutions of 0.1 mg.ml^{-1}).

In addition, the various PPMLs were immunostained with an antibody against Fbg for identifying the differences in the amount of the attached Fbg on the glass. Confocal microscopy analysis showed that all the combinations of PPMLs contain a high amount of Fbg (**Figure 3**). The fluorescent intensity of Fbg is higher when it corresponds to the last deposited layer, which indicates a degree of separation between the sequentially deposited layers (**Figure 3b,d**). In addition, the fluorescent intensity of Fbg is higher when the solution concentration is higher (**Figure 3d**). The Fbg layer appears to be less uniform in the case of PPMLs with Chit as last layer obtained using the lower concentration, **leading to the speculation that** interdiffusion of Fbg and Chit layers took place (**Figure 3a**). These interpenetrated layered structures are in accordance to the literature, indicating that immersive LbL assembly leads to films that grow in a nonlinear manner [57,58]. This strong interpenetration possibly allows the formation of network structures consisting of Fbg molecules which could explain the morphology observed in Figure 3a. In any case confocal microscopy with immunostained Fbg proves the successful deposition of PPMLs on the glass substrate and illustrates the tunability of the adsorbed amount (**see movies, SI**).

The information derived from fluorescence microscopy can be useful for identifying the optimized coating amount for efficient cell culture. Combining the results of FT-IR and contact angles with the confocal images, it seems that the PPMLs with higher concentration can very possibly lead to the same amount of deposited Chit and Fbg. Aiming to scrutinize the synergistic effect of Chit and Fbg, we proceeded with the cell culture studies using the PPMLs having Chit as last layer (**Figure 3a, c**). In this case, there are most certainly Chit segments exposed to the exterior. As the layers appear mixed, Fbg units are possibly also exposed to the external medium. Therefore, in the particular PPMLs (with Chit as the last added layer) both biopolymers certainly affect cell-PPML interactions.

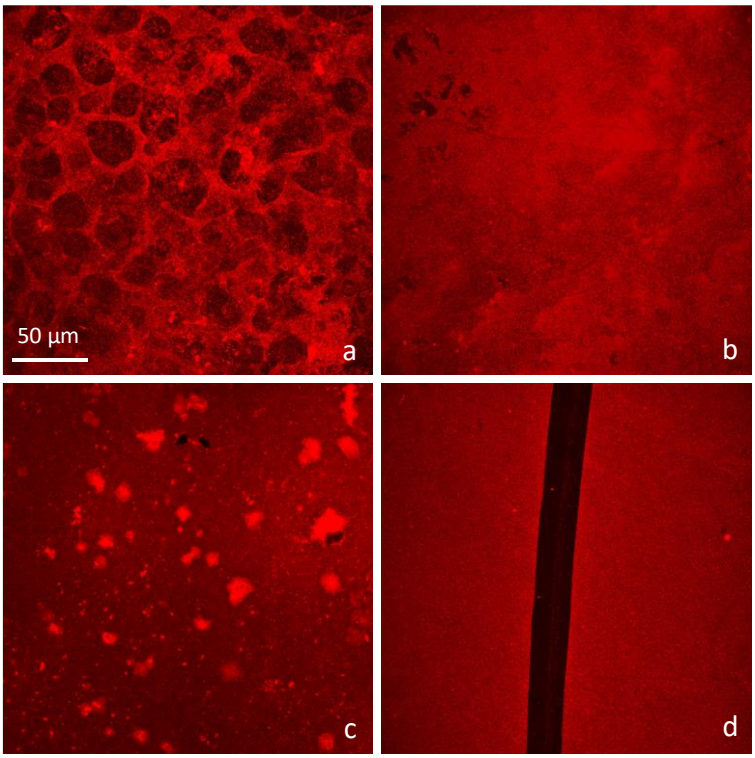

Figure 3. Fluorescent images of Fbg on the different PPMLs of five alternating bilayers from solutions of 0.1 mg.ml^{-1}: Fbg (a), Chit (b) as the first layer and 1 mg.ml^{-1}: Fbg (c), Chit (d) as the first layer (the sample was scratched, for this reason the dark area appears).

3.2. Cardiomyocytes cytocompatibility on PPMLs

The cytocompatibility of both Chit and Fbg has been reported in various studies using different cell types [25,26,59]. Nevertheless, the combination of both biomaterials as coating for cell culture has not yet been explored. In this work, we aimed at scrutinizing the interaction of these PPMLs with cardiomyocytes. It has to be pointed out that cardiomyocytes do not adhere, consequently do not survive, in pure glass without a coating. In addition, this type of cells does not proliferate, rendering their successful culture challenging. Herein, we cultured primary cardiomyocytes (NRCMs) for 3 days on the surface of all samples and then we assessed their viability and morphology. Pure glass lamella served as control in addition to laminin coating, which is the most common used for NRCMs culture.

Before comparing the effect of multiple layers of Chit/Fbg on cell viability, we cultured NRCMs on single layers of Chit and Fbg with concentrations 0.1 and 1 mg.ml^{-1}. NRCMs

survival was extremely low on the surfaces with one layer of Chit (**Figure 4a-b**). This result is in accordance with the literature, where poor NRCMs adhesion with rounded morphology was observed when cultured on Chit surfaces [60]. On the contrary, a single layer of Fbg was sufficient for the attachment and spreading of NRCMs, even at the lower concentration, indicating its strong adsorption to the glass substrate (**Figure 4c-d, 5**).

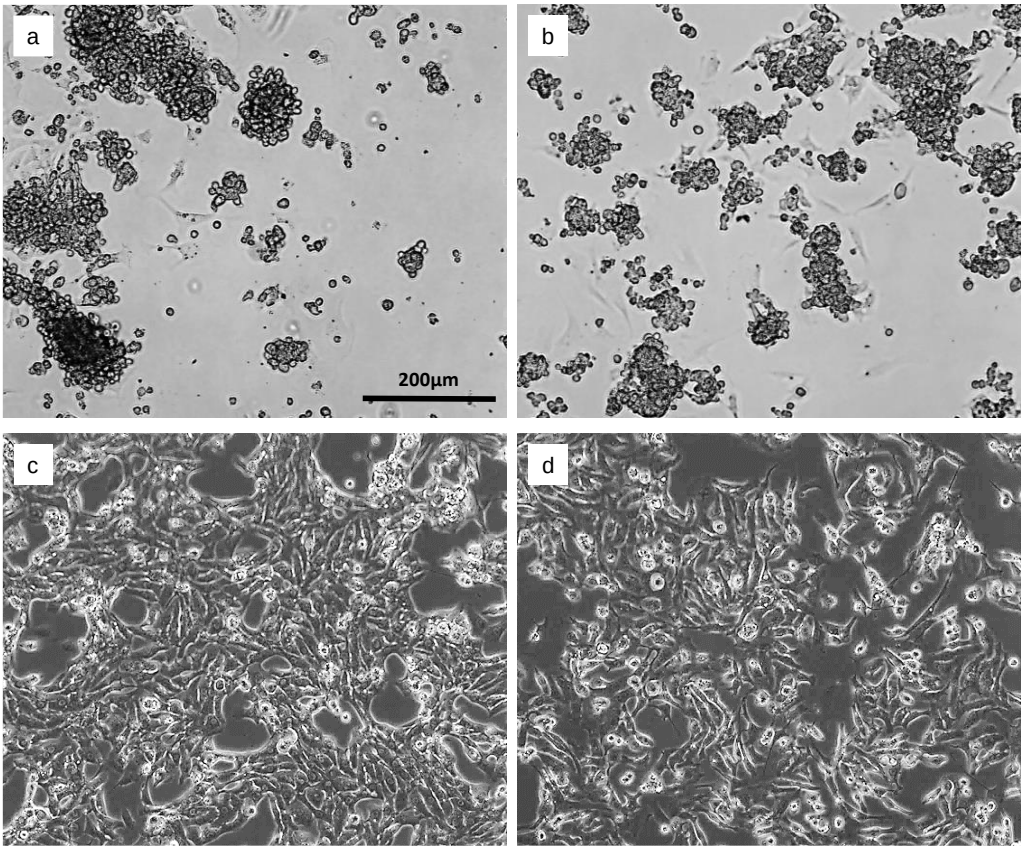

Figure 4. Optical live images of NRCMs seeded on single layers of Chit (a, b) and Fbg (c, d) with concentrations of 0.1 (a, c) and 1 (b, d) $mg.ml^{-1}$ respectively.

As demonstrated in **Figure 5**, the live cells were quantified using the Muse® Count & Viability Kit and showed that their number is high for all coatings, except for single layers of Chit. In the latter, their number was as low as in the bare glass, confirming the results in **Figure 4**. The statistical analysis has shown that there is a significant difference between bare glass and the following: laminin, Fbg_high, PPMLs_low, PPMLs_high. The viability of laminin is at the

same levels of single layers of Fbg and PPMLs. The PPML with high concentration exhibited higher viability, even though this difference is not significant when compared with laminin.

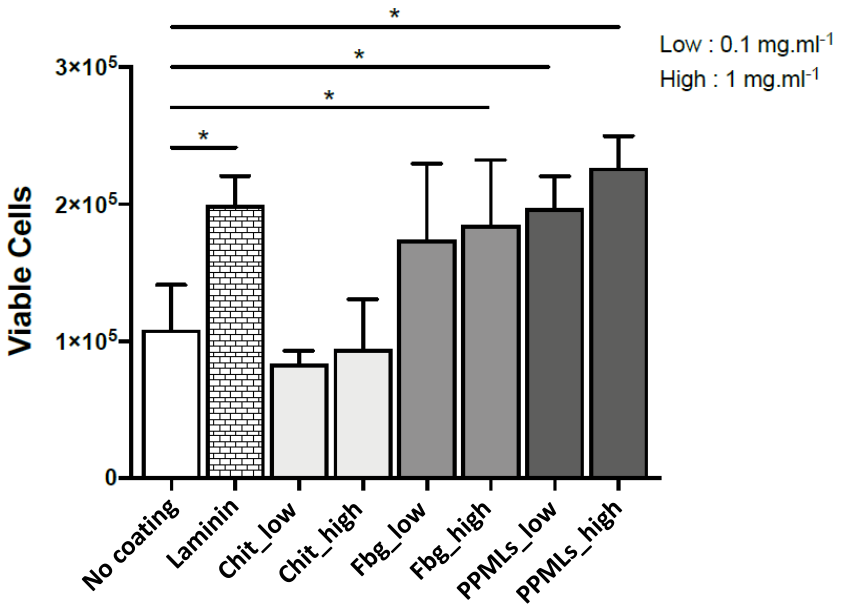

Figure 5. Viability results of NRCMs cultured on single layers (1L) of Chit and Fbg with concentrations of 0.1 (low) and 1 (high) mg.ml^{-1} and on PPMLs with Fbg as first layer and concentrations of 0.1 (low) and 1 (high) mg.ml^{-1}, compared with laminin coating and bare glass lamellae.

We further assessed the cytocompatibility of PPMLs in terms of cell morphology employing immunofluorescence. Confocal microscopy analysis of cultured NRMCs on coated glass showed that they have an elongated shape, close to the in vivo one (**Figure 6**). While the small number of cells that attached and survived on glass lamella presented round shape with short bundles of α-actinin (**Figure 6a**). Among the various coatings, the PPML with Fbg as first layer with high concentration showed better-defined striations of sarcomeres as indicated by α-actinin immunostaining (**Figure 6f,h**). For better visualization of the sarcomeres, the **Figure 6g,h** shows magnified confocal images of cells stained with phalloidin together with α-actinin immunolabelling on laminin-coated and PPMLs of 1mg.ml^{-1} samples. Phalloidin stains the actin filaments, which consist part of the sarcomere together with myosin II filaments [61]. It is obvious that laminin coating did not lead to the creation of well-structured striations of the sarcomeres as in the case of PPMLs of 1mg.ml^{-1}. A well-constructed sarcomere is key element

for the function of cardiomyocytes as it consists their contractile unit [62], and is of paramount importance when developing in vitro cardiac models. As cardiac contractile performance is highly dependent on sarcomere length (SL), we calculated the latter and compared it to the literature [63]. The SL of NRCMs cultured on PPML with high concentration is 1.72 ± 0.2 μm, which is within the range of the reported values (**Figure S1**) [64–66]. The obtained SL (1.61 ± 0.54 μm) upon culture on laminin coating is not only lower but also exhibits high variation, thus further validating the results of immunofluorescence. Combining these observations with the viability results, we can conclude that the PPML with Fbg as first layer and concentration of 1mg.ml^{-1} is the most suitable coating for the culture of NRCMs.

Therefore, these findings can be used for the functionalization of scaffolds based on polycations with Fbg via LbL assembly. In this way a composite material will be created combining favourable properties of both biomaterials, which is a key parameter in cardiac tissue engineering [67]. The multilayer structure and internally modulated hydrophilicity of the composite coatings allows for the entrapment of various active components that could be beneficial for the differentiation of cells. In addition, LbL construction including Chit provides a means to tune the adsorbed amount of Fbg and a quasi-3D structure to the adsorbed films.

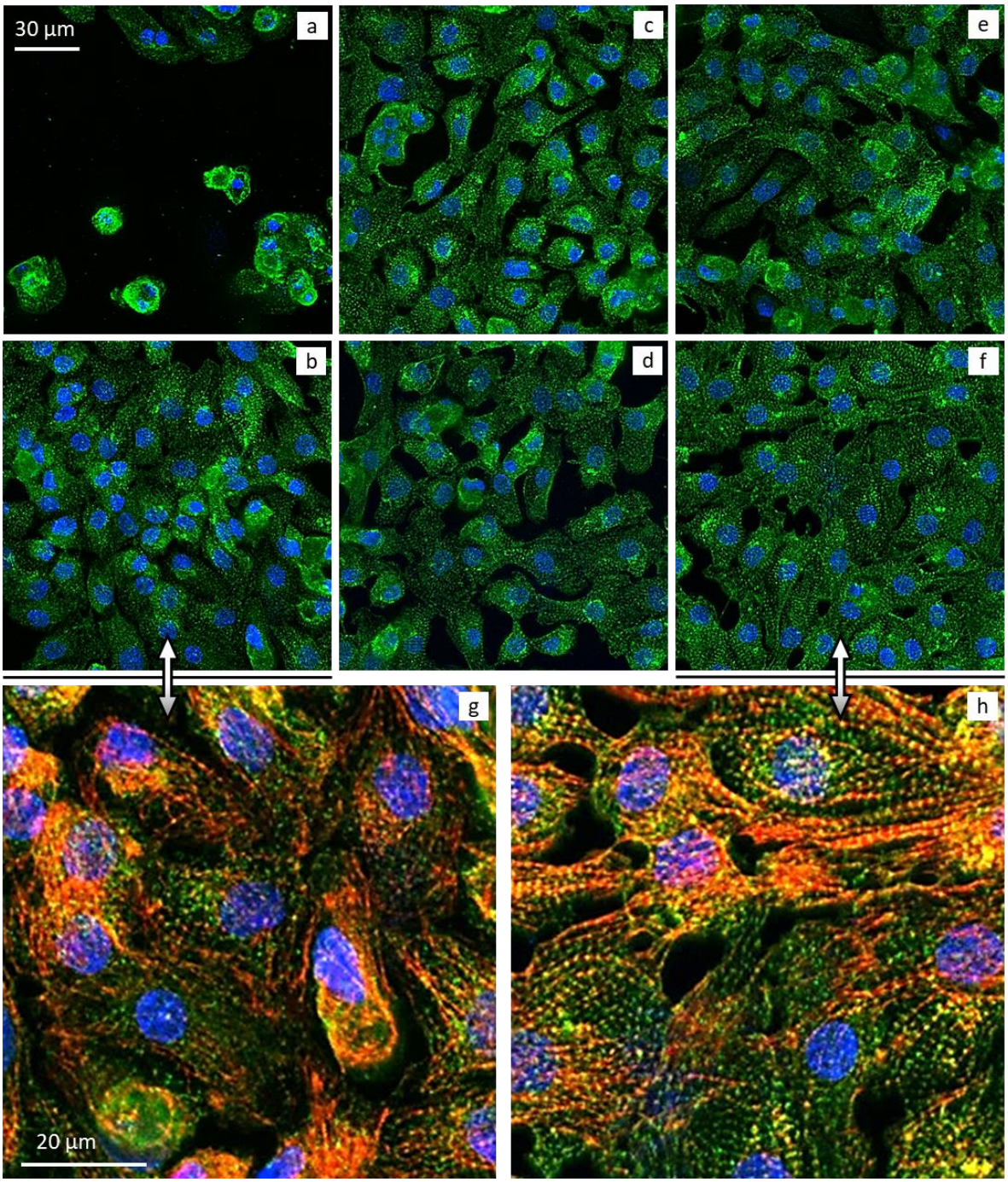

Figure 6. Confocal images of NRCMs seeded on: glass lamella (a) and laminin coating (b), single layers of Fbg with concentrations of 0.1 (c) and 1 (d) $mg.ml^{-1}$, PPMLs with Fbg as first layer and concentrations of 0.1 (e) and 1 (f) $mg.ml^{-1}$. (g)-(h): zoomed images of (b) and (f), respectively. Scale bar a-f: 30µm, g-h: 20µm. Green: α-actinin, red: phalloidin, blue: nuclei.

3. Conclusion

We investigated two approaches in LbL assembly for unmasking the optimal PPMLs combination that leads to improved cardiomyocytes viability and morphology: the bilayers

order namely the coating that is in contact with the cell surface, and the biopolymers' concentration. Concentration increase was found to enhance the amount of adsorbed protein while it reduced the degree of mixing between the successive layers. The choice of the biopolymer that was added on top was found to influence the hydrophilicity of the Chit/Fbg coating as Chit led to more hydrophilic layers in comparison to Fbg. Pure Fbg coating was sufficient for good NRCMs adhesion and spreading, but NRCMs morphology is superior when cultured on 5 bilayers of PPMLs of 1 $mg.ml^{-1}$ concentration. This result was further confirmed by the value of sarcomere length (SL), which is a key determinant of cardiac mechanical function. Additionally, the presence of Chit facilitates the tuning of Fbg adsorbed amount and the incorporation of other bioactive compounds that could bind to Fbg. These findings are useful for the optimization of the surface properties of biomaterials that can be applied to cardiac tissue engineering. For example, synthetic scaffolds can be functionalized by the proposed LbL assembly for enhancing their cytocompatibility. In addition, these PPMLs exhibited long shelf-life, which increases the versatility of their use in cell cultures.

4. Experimental Section

Materials: Chit (low molecular weight, 75-85% deacetylated) and Fbg from bovine plasma (type I-S, 65-85% protein) were purchased from Sigma and were used without further treatment. Stock solutions of Chit (1 $mg.ml^{-1}$) or Fbg (10 $mg.ml^{-1}$) were prepared by dissolving the Chit powder in aqueous solution of acetic acid (pH 5) and Fbg in a 0.15 M NaCl solution (pH 7) and were left overnight at 4 °C to equilibrate. Solutions at lower concentrations were prepared by diluting the stock solutions with their aqueous solvents. Laminin (L2020, 1-2 $mg.ml^{-1}$ in Tris buffered NaCl) was purchased from Sigma-Aldrich and was stored at -20°C. Before use, laminin was diluted in Dulbecco's phosphate buffer saline (DPBS) (Thermo Fisher Scientific, Saint-Herblain, France), in order to obtain a final concentration of 0.02-0.04 $mg.ml^{-1}$.

Formation of polysaccharide/protein multilayers (PPMLs) based on the Chit/Fbg pairs: Films of alternating Chit/Fbg were deposited on glass lamellae by the LbL deposition method. Briefly, fresh glass lamellae were rinsed with distilled water and dried under nitrogen stream to remove any dust particles. A glass lamella of 12mm-diameter was immersed vertically in the solution of Chit or Fbg for 5 min before it was gently rinsed with water in order to remove material that was not adsorbed on the surface. The procedure was repeated for the other macromolecule i.e. Fbg or Chit respectively, until five pairs (bilayers) were deposited. Two different solution concentrations were used for Chit and Fbg: 0.1 and 1.0 mg/ml to prepare Chit/Fbg multilayers. The samples were dried at room temperature and then were stored at 4^0C until use. The coatings were stable even after six months of storage indicating their long shelf-life. For the control experiments with laminin, the coatings were prepared just before the cell culture. The diluted laminin solution was deposited on top of the glass lamellae for 2 h at room temperature, followed by a wash with DPBS.

FTIR experiments*:* FTIR measurements were realized on gold-coated microscope slides. The LbL deposition was performed on a commercial gold-coated (100 nm) microscopy slide. An attenuated total reflectance (ATR) diamond accessory, from SENS-IR, and a press were used to record Infrared spectra on a Bruker Equinox 55 Fourier Transform Instrument. Two measurements were taken from different spots of the glass slides placed at the center of the sample holding device and 64 scans were performed in the range 500-5,000 cm^{-1}, at a resolution of 2 cm^{-1}.

Contact angle (CA) experiments: CA measurements of water sessile drops were performed, using a custom-made experimental set-up, on the glass lamellae that were utilized for the cell studies. Images of 5 μL water drops on the surface of each substrate after rinsing with water were obtained by a 2.0MP 500x USB Digital Microscope within 30 s from the droplet deposition. The drop profiles were analyzed by standard MATLAB functions. In brief, the drop edge profile was determined after transforming the images to grayscale. For numerical

calculations the origin of the coordinates was chosen on the intersection between the apparent perpendicular axis of symmetry of the drop and the solid/liquid interface. Edge profiles were treated in polar coordinates (r, θ) because $r(\theta)$ varies smoothly with θ and is hence effectively fitted by polynomial functions. The values of CA were extracted from the derivatives on the left and right-side contacts of the drop with the surface and transformed back to Cartesian coordinates. The average of the two values from different spots on the glass lamella was reported as the measured CA. Typically, the deviation between left and right contact angles was less than 2° and their average was taken as the CA for the particular sessile drop. The CAs were measured at room temperature.

Isolation of neonatal rat cardiomyocytes: Newborn rat cardiomyocytes (NRCMs) were obtained from 1-day-old Wistar RjHan rat (Janvier Labs, Saint-Berthevin, France). The hearts were cut in small pieces and the cardiac cells were isolated, using a neonatal heart dissociation kit (Miltenyi Biotec, Paris, France) according to the manufacturer's instructions. Cardiomyocytes were purified by depletion of non-target cells (such as fibroblasts, endothelial cells), using a neonatal cardiomyocyte isolation kit (Miltenyi Biotec, Paris, France). 5 x 10^5 cells were seeded on glass lamellae of 12mm-diameter coated with the PPMLs and cultured with DMEM medium (with 4.5g/L D-Glucose and without Na Pyruvate) supplemented with L-glutamine, penicillin-streptomycin, 10% horse serum and 5% fetal bovine serum (FBS) at 37 °C and 5% CO_2 for 3 days.

All procedures were performed in accordance with national and European legislations, in conformity with the Public Health Service Policy on Human Care and Use of Laboratory Animals under the license C75.05.24. All animal studies were approved by our institutional Ethics Committee "Charles Darwin" and conducted according to the French and European laws, directives, and regulations on animal care (European Commission Directive 2010/ 63/EU).

Immunostaining and cell morphology analysis: For the Fbg immunostaining, PPMLs samples without cells were immunostained using an antibody against Fbg (rabbit polyclonal

antibody, dilution 1:200, Bioss Antibodies). After 3 washes in PBS, the samples were mounted with mowiol.

The NRCMs, cultured on PPMLs and controls, were washed with PBS and fixed with 4% paraformaldehyde solution. After 3 washing steps, they were incubated with 5% bovine serum albumin (BSA) containing 0,1 % Triton X-100 for 1 hour. The cells were incubated for 90 minutes at room temperature with an antibody against α-actinin (mouse IgG, dilution 1:300, Sigma-Aldrich, Saint-Quentin-Fallavier, France). After 3 washes in PBS, cells were incubated in the presence of the secondary antibody (Alexa 488 goat-anti-mouse) and Alexa Fluor® 647 phalloidin (Life technologies). Then samples were mounted with mowiol containing 5 µg/ml Hoescht 33342 (Life Technologies).

All images were captured using a motorized confocal laser scanning microscope (Leica TCS SP5). Sarcomere length (SL) was measured by α-actinin immunostaining using ImageJ.

Viability assay: The viability of NRCMs was assessed by using the Muse® Count & Viability Kit. The kit differentially stains viable and non-viable cells based on their permeability to the two DNA binding dyes present in the reagent. The measurements were repeated at least 3 times, using 3 samples per time.

Statistics: Analyses were conducted using GraphPad Prism 8.00 (GraphPad Software Inc., SD, USA). For one-way analysis of variance, the normality was checked using the Shapiro-Wilk normality test. If the normality of distribution assumption was not met, the nonparametric Kruskal-Wallis test was used instead of ANOVA. If a significant difference was found, then multiple comparison tests were performed to compare the different groups analyzed by controlling the False Discovery Rate. A p-value < 0.05 was considered significant. Values are given as the means ± standard error of the mean.

Supporting Information

Supporting Information is available from the Wiley Online Library or from the author.

Acknowledgements

The authors thank Dr. Georgios D. Chryssikos and Dr. Eirini Siranidi for their help in ATR-FTIR measurements. The authors also thank the personnel of the Photon Microscopy Facility of IBPS for helpful advice and technical assistance during microscopy image acquisition and analysis. This work was supported by the LabEx REVIVE (ANR-10-LABX-73). Also, this work has been sponsored by the Ile-de-France Region in the framework of Respore, the Île-de-France network of Excellence in Porous Solids". MK acknowledges personal funding from both LabEx REVIVE and DIM Respore too.

Conflicts of interest

There are no conflicts to declare.

References

1. V. Gribova, R. Auzely-Velty, C. Picart, *Chem. Mater.* **2012**, *24*, 854.
2. A. J. Nathanael, T. H. Oh, *Polymers (Basel).* **2020**, *12*, 1.
3. J. Zeng, M. Matsusaki, *Polym. Chem.* **2019**, *10*, 2960.
4. L. Séon, P. Lavalle, P. Schaaf, F. Boulmedais, *Langmuir* **2015**, *31*, 12856.
5. V. A. Izumrudov, B. K. Mussabayeva, K. B. Murzagulova, *Russ. Chem. Rev.* **2018**, *87*, 192.
6. P. T. Hammond, *Adv. Mater.* **2004**, *16*, 1271.
7. A. B. Kayitmazer, D. Seeman, B. B. Minsky, P. L. Dubin, Y. Xu, *Soft Matter* **2013**, *9*, 2553.
8. F. Comert, A. J. Malanowski, F. Azarikia, P. L. Dubin, *Soft Matter* **2016**, *12*, 4154.
9. A. vander Straeten *et al.*, *Nanoscale* **2017**, *9*, 17186.
10. M. J. Landry *et al.*, *Macromol. Biosci.* **2019**, *19*, 1900036.
11. S. Zhang, M. Xing, B. Li, *Int. J. Mol. Sci.* **2018**, *19*, 1641.
12. Y. M. Baba Ismail, A. M. Ferreira, O. Bretcanu, K. Dalgarno, A. J. El Haj, *Colloids Surfaces B Biointerfaces* **2017**, *159*, 445.
13. B. Li, *Nanotechnol. Sci. Appl.* **2009**, *Volume 2*, 21.
14. I. Ding, D. M. Shendi, M. W. Rolle, A. M. Peterson, *Langmuir* **2018**, *34*, 1178.
15. N. E. Muzzio *et al.*, *Macromol. Biosci.* **2016**, *16*, 482.

16. N. E. Muzzio, M. A. Pasquale, S. E. Moya, O. Azzaroni, *Biointerphases* **2017**, *12*, 04E403.
17. T. Boudou, T. Crouzier, C. Nicolas, K. Ren, C. Picart, *Macromol. Biosci.* **2011**, *11*, 77.
18. K. Kadowaki, M. Matsusaki, M. Akashi, *Langmuir* **2010**, *26*, 5670.
19. F. Croisier, C. Jérôme, *Eur. Polym. J.* **2013**, *49*, 780.
20. J. Berger, M. Reist, J. . Mayer, O. Felt, R. Gurny, *Eur. J. Pharm. Biopharm.* **2004**, *57*, 35.
21. A. Banerjee, S. Ganguly, *J. Appl. Polym. Sci.* **2019**, *136*, 47599.
22. G. Cárdenas, P. Anaya, C. von Plessing, C. Rojas, J. Sepúlveda, *J. Mater. Sci. Mater. Med.* **2008**, *19*, 2397.
23. S. Boddohi, N. Moore, P. A. Johnson, M. J. Kipper, *Biomacromolecules* **2009**, *10*, 1402.
24. S. Kattula, J. R. Byrnes, A. S. Wolberg, *Arterioscler. Thromb. Vasc. Biol.* **2017**, *37*, e13.
25. S. A. Sell *et al.*, *Biomed. Mater.* **2008**, *3*, 045001.
26. D. Gugutkov, J. Gustavsson, M. P. Ginebra, G. Altankov, *Biomater. Sci.* **2013**, *1*, 1065.
27. S. S. A. An, Rajangam, *Int. J. Nanomedicine* **2013**, *8*, 3641.
28. W. Xu, D. W. Chung, E. W. Davie, *J. Biol. Chem.* **1996**, *271*, 27948.
29. S.-Y. Jung *et al.*, *J. Am. Chem. Soc.* **2003**, *125*, 12782.
30. M. Wasilewska, Z. Adamczyk, B. Jachimska, *Langmuir* **2009**, *25*, 3698.
31. D. Forciniti, W. A. Hamilton, *J. Colloid Interface Sci.* **2005**, *285*, 458.
32. J. Koo *et al.*, *Biomacromolecules* **2012**, *13*, 1259.
33. Y. Hu *et al.*, *Langmuir* **2016**, *32*, 4086.
34. T. A. Horbett, *J. Biomed. Mater. Res. Part A* **2018**, *106*, 2777.
35. H. P. Felgueiras *et al.*, *ACS Appl. Mater. Interfaces* **2016**, *8*, 13207.
36. R. Novoa-Carballal, R. Riguera, E. Fernandez-Megia, *Polymer (Guildf).* **2013**, *54*,

2081.

37. N. Boucard *et al.*, *Biomacromolecules* **2007**, *8*, 1209.
38. K. Kubiak, Z. Adamczyk, M. Cieśla, *Colloids Surfaces B Biointerfaces* **2016**, *139*, 123.
39. T. T. M. Ho *et al.*, *Langmuir* **2015**, *31*, 11249.
40. G. Lawrie *et al.*, *Biomacromolecules* **2007**, *8*, 2533.
41. S. Rodrigues, A. M. R. da Costa, A. Grenha, *Carbohydr. Polym.* **2012**, *89*, 282.
42. P. Schwinté *et al.*, *J. Phys. Chem. B* **2001**, *105*, 11906.
43. M. Boix *et al.*, *J. Biomed. Mater. Res. Part A* **2015**, *103*, 3493.
44. Y. Liu, S. Wang, R. Zhang, *Int. J. Biol. Macromol.* **2017**, *103*, 1130.
45. A. Regiel-Futyra *et al.*, *RSC Adv.* **2017**, *7*, 52398.
46. T. Parandhaman, N. Pentela, B. Ramalingam, D. Samanta, S. K. Das, *ACS Sustain. Chem. Eng.* **2017**, *5*, 489.
47. M. Salim, B. O'Sullivan, S. L. McArthur, P. C. Wright, *Lab Chip* **2007**, *7*, 64.
48. J. Armstrong *et al.*, *J. Phys. Condens. Matter* **2004**, *16*, S2483.
49. E. Poptoshev, P. M. Claesson, *Langmuir* **2002**, *18*, 1184.
50. J. Nilsen-Nygaard, S. Strand, K. Vårum, K. Draget, C. Nordgård, *Polymers (Basel).* **2015**, *7*, 552.
51. D. Sriramulu, E. L. Reed, M. Annamalai, T. V. Venkatesan, S. Valiyaveettil, *Sci. Rep.* **2016**, *6*, 35993.
52. R. Dineshram *et al.*, *Colloids Surfaces B Biointerfaces* **2009**, *74*, 75.
53. C. J. van Oss, *J. Protein Chem.* **1990**, *9*, 487.
54. D. W. Lee, C. Lim, J. N. Israelachvili, D. S. Hwang, *Langmuir* **2013**, *29*, 14222.
55. Q. Tan, Y. Kan, H. Huang, W. Wu, X. Lu, *Coatings* **2020**, *10*, 1052.
56. S. Amine, A. Montembault, M. Fumagalli, A. Osorio-Madrazo, L. David, *Polymers (Basel).* **2021**, *13*, 2023.
57. P. Lavalle *et al.*, *J. Phys. Chem. B* 2004, *108*, 635.

58. V. Z. Prokopović, C. Duschl, D. Volodkin, *Macromol. Biosci.* 2015, *15*, 1357.

59. I.-Y. Kim *et al.*, *Biotechnol. Adv.* **2008**, *26*, 1.

60. A. Hussain, G. Collins, D. Yip, C. H. Cho, *Biotechnol. Bioeng.* **2013**, *110*, 637.

61. A. M. Fenix *et al.*, *Elife* **2018**, *7*, 1.

62. Y. Au, *Cell. Mol. Life Sci.* **2004**, *61*, 3016.

63. P. P. de Tombe, H. E. D. J. ter Keurs, *J. Mol. Cell. Cardiol.* **2016**, *91*, 148.

64. G. Bub *et al.*, *Am. J. Physiol. - Hear. Circ. Physiol.* **2010**, *298*.

65. L. Burbaum *et al.*, *bioRxiv* **2020**, 1, doi:10.1101/2020.09.09.288977.

66. P. Peterson, M. Kalda, M. Vendelin, *Am. J. Physiol. - Cell Physiol.* **2013**, *304*, 519.

67. M. Kitsara, O. Agbulut, D. Kontziampasis, Y. Chen, P. Menasché, *Acta Biomater.* **2017**, *48*, 20.